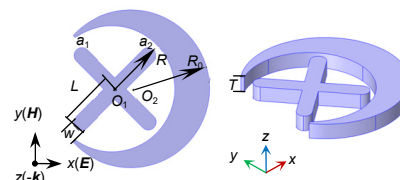




DOI: 10.12086/oe.2020.200010

# Generation of multiple Fano resonance and high FOM resonance based on the crescent cross nanostructure



Hou Yibo, Huo Yiping\*, Jiang Xueying, Zhou Chen, Guo Yiyuan,  
Niu Qiqiang, He Qian, Hao Xiangxiang

School of Physics and Information Technology, Shaanxi Normal University, Xi'an, Shaanxi 710062, China

**Abstract:** Metal surface plasmon has many novel optical properties and important applications, and it is also a research hotspot. In this paper, a crescent cross (CC) nanostructure composed of a crescent and a cross is studied by the finite element method. New plasmon magnetic mode and multiple Fano resonance can be induced by breaking structure symmetry through changing structure parameters. Meanwhile, by changing the angle between the two rods symmetrically, the figure of merit (FOM) can reach 61. Our structure has important applications in the fields of multi-wavelength sensor, ultra-sensitive biosensor, surface enhanced spectroscopy, and slow light transmission.

**Keywords:** multiple Fano resonance; surface plasmon; figure of merit

**Citation:** Hou Y B, Huo Y P, Jiang X Y, *et al.* Generation of multiple Fano resonance and high FOM resonance based on the crescent cross nanostructure[J]. *Opto-Electronic Engineering*, 2020, **47**(11): 200010

## 新月十字架纳米结构中多 Fano 共振的产生和高 FOM 共振

侯艺博, 霍义萍\*, 姜雪莹, 周 辰, 郭懿圆, 牛启强, 何 倩, 郝祥祥

陕西师范大学物理学与信息技术学院, 陕西 西安 710062

**摘要:** 金属表面等离激元具有许多新颖的光学特性和重要的应用, 并且也是当今研究的热点。本文采用有限元方法研究了由新月和十字架组成的新月十字架纳米结构。通过改变结构参数来打破结构对称性, 可以产生新的等离激元磁模式和多重 Fano 共振。同时, 通过对称地改变两棒之间的夹角, FOM 值可以达到 61。我们的结构在多波长传感器、超灵敏生物传感器、表面增强光谱和慢光传输等领域有着重要的应用。

**关键词:** 多 Fano 共振; 表面等离激元; 品质因数

中图分类号: TP212

文献标志码: A

引用格式: 侯艺博, 霍义萍, 姜雪莹, 等. 新月十字架纳米结构中多 Fano 共振的产生和高 FOM 共振[J]. 光电工程, 2020, **47**(11): 200010

收稿日期: 2020-01-06; 收到修改稿日期: 2020-03-31

基金项目: 国家自然科学基金资助项目(11604198)

作者简介: 侯艺博(1995-), 男, 硕士, 主要从事表面等离激元光子学的研究。E-mail: hou994682946@qq.com

通信作者: 霍义萍(1977-), 女, 博士, 副教授, 主要从事表面等离激元光子学的研究。E-mail: yphuo@snnu.edu.cn

版权所有©2020 中国科学院光电技术研究所

## 1 Introduction

In recent years, great progress has been made in the research based on surface plasmons (SPs). SPs has been widely used in nano-optoelectronic integration, optical imaging, biosensor, data storage, and has attracted great attention of researchers<sup>[1-2]</sup>. SPs is collective charge oscillation existing at the interface between conductor and dielectric. SPs is an electromagnetic wave in essence<sup>[3]</sup>, and it can be divided into two types: one is propagating surface plasmon polaritons (SPPs), which can propagate along the interface between metal and dielectric; the other is limited by metal nanostructure and can only be confined to the surface of metal nanoparticles, which is called local surface plasmons (LSPs). SPs are favored by researchers for it can manipulate and integrate photons at micro-nanoscale<sup>[4]</sup>. SPs not only can enhance the local electromagnetic field on the metal surface, but also break the optical diffraction limit, thus realizing the nanometer-scale regulation of light field<sup>[5]</sup>. SPs have extremely important application value in related aspects due to their novel optical properties, such as plasmon waveguides<sup>[6]</sup>, surface enhanced Raman scattering<sup>[7]</sup>, electromagnetic induced transparency, and Fano resonance effect<sup>[8-9]</sup>.

Fano resonance comes from the quantum system originally. When the discrete and the continuous energy level are superimposed, quantum interference occurs and low absorption happens at a specific optical frequency, which results in an asymmetric linetype. U Fano explained the mechanism of asymmetric linetype by using strict theory<sup>[10-11]</sup>. In the SPs system, Fano resonance can be formed by the coupling between the bright mode (superradiant) and the dark mode (subradiant), which results in the asymmetric spectrum<sup>[12]</sup>. Fano resonance is characterized by asymmetric linetype. A spectral dip is formed through coupling of bright mode and dark mode, where scattering is suppressed and absorption is enhanced<sup>[13-14]</sup>. The bright mode has a large net dipole moment, which can be excited directly by incident light and exhibits a wider line-width spectrum<sup>[14-15]</sup>. The net dipole moment of dark mode is almost zero, so it has a small radiation damping and shows a narrow line width<sup>[14-16]</sup>. Different from the bright mode, dark mode can only be excited by near-field coupling or symmetry breaking<sup>[13,17]</sup>. For example, Zhu's team studied the structure of silver nanorods with wedge-shaped parts, the Fano line shape arises from the coupling between a hybridized plasmon resonance of the disk and a narrower quadrupolar mode supported by the edge of the missing wedge slice. Fang's team made the structure of heptamer graphene type light probe, where the structure of heptamer is intermingled in the middle of monolayer graphene and Fano resonance is formed through the coupling of heptamer and graphene<sup>[13-14]</sup>. The radiation loss of Fano resonance is small, and the energy of the incident field can be better confined to the structure surface<sup>[18-20]</sup>. Based on these optical properties, Fano resonance effect can be widely used in

biosensors<sup>[21]</sup>, electromagnetic induction absorption<sup>[22]</sup>, optical switches<sup>[23]</sup>, photodetectors<sup>[24-25]</sup>, etc.

Due to the lack of natural magnetism, people initially focused on electric Fano resonance. However, the magnetic Fano resonance has advantages that the electrical Fano resonance does not have. A closed-loop current can be formed, which can limit the energy more locally, reduce the scattering loss, and strengthen the response of the magnetic field<sup>[26-27]</sup>. In nanostructures, artificial optical magnetism can be obtained by breaking the symmetry of nanostructure to form magnetic Fano resonance. The obvious characteristic of magnetic Fano resonance is a closed current loop. These features and advantages make magnetic Fano resonances have great potential application in metamaterials, stealth, and high-resolution lithography<sup>[28]</sup>. When the structure symmetry is destroyed, due to the generation of high order dark state, multiple Fano resonance effect can be induced<sup>[29]</sup>. Compared with single Fano resonance, multiple Fano resonance effects can adjust multiple waveband spectrum simultaneously<sup>[30-31]</sup>. The nanostructure parameter effects the modulation depth and resonance frequency of multiple Fano resonance greatly<sup>[32]</sup>. In addition, the spectrum of Fano resonance varies with the refractive index of environment, which is very suitable for sensing applications<sup>[32-33]</sup>. Many studies have been carried out to improve the figure of merit (FOM), which can measure the sensing properties of the structure. For example, the maximum FOM of the T-type nanorod dimer structure proposed by Feng team is 9.5<sup>[34]</sup>; the FOM value of Hu team's I-type trimer structure with two rods can reach 25.9<sup>[35]</sup>; the FOM value of the H-type nanostructure designed by Goncalves team is 30<sup>[36]</sup>.

The split ring is one of the most common structure in the study of plasmon. A cross is added on the split ring nanostructure, and the cross can be rotated, so the structure asymmetry degree can be adjusted conveniently in various ways. In theory, the cross and the crescent are coupled to form a magnetic pattern and generate magnetic Fano resonance. New plasmon modes and multiple Fano resonance can be induced by breaking structure symmetry through changing structure parameters. In addition, the FOM value can be modulated by changing the angle between two rods symmetrically and the maximum FOM value reaches 61. These optical properties make our structure have broad application prospects in surface enhanced Raman scattering, plasmon scale, multi-band sensing, etc.

## 2 Structure and simulation method

Figure 1 shows 2-D and 3-D views of the CC nanostructure. The cross is composed of bar  $a_1$  and bar  $a_2$ . The centers of the inner ring and the outer ring are  $O_1$  and  $O_2$ , respectively. The radius of the inner ring and outer ring are  $R$  and  $R_0$ , respectively. The width and half length of the nanorods are  $w$  and  $L$ , respectively. The thickness of

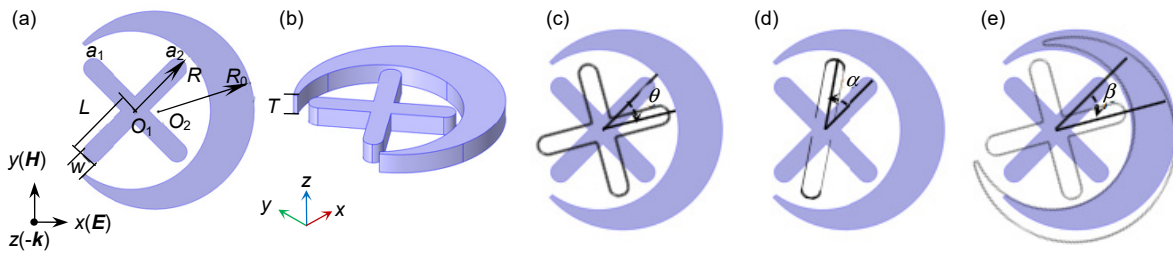


Fig. 1 (a) 2-D structure and geometric parameters of the CC nanostructure; (b) 3-D schematic diagram of the CC nanostructure; The rotation angles of the cross (c), rod  $a_2$  (d) and the whole structure (e) around  $O_1$ , are  $\theta$ ,  $\alpha$  and  $\beta$  degrees respectively

the whole nanostructure is  $T$ . Figs. 1(c)~1(e) are the rotation angles of the cross, rod  $a_2$  and the whole structure around  $O_1$ , which are  $\theta$ ,  $\alpha$  and  $\beta$  respectively. The light incident along the negative  $z$  axis and the polarization direction is along  $x$  axis. Compared with other metal materials, silver has the lower loss in the visible light, so silver is selected as the material of the CC nanostructure. The dielectric constant of silver is taken from Johnson and Christy (JC), and the surrounding medium is air.

In this paper, a commercial software COMSOL Multiphysics based on the finite element method is used to calculate the optical response of the CC nanostructure. The extinction cross section of the CC nanostructure is calculated, which is equal to the sum of the absorption cross section and the scattering cross section. The total scattering cross section is calculated by integrating the scattered power flux on the outer closed surface of the CC nanostructure. A spherical perfect matching layer (PML) was designed to eliminate the interference of boundary reflections and absorb all of the emitted radiation.

### 3 Results and discussion

#### 3.1 Optical response characteristic of the CC nanostructure

Fig. 2(a) shows the extinction spectrum of the CC nano-

structure, where  $R=80$  nm,  $R_0=100$  nm,  $L=60$  nm,  $w=20$  nm and  $T=20$  nm. From the left to the right, there are three resonance peaks, which are named  $E'$ ,  $E$  and  $M$ . A Fano dip  $m$  is formed between  $E$  and  $M$ . In order to explore the formation of this Fano dip, we give the charge distributions, surface current density and magnetic field enhancement distributions of peak  $E'$ ,  $E$ ,  $M$  and dip  $m$ . Figs. 2(b)~(e) show the charge distributions of  $E'$ ,  $E$ ,  $m$  and  $M$ , and Figs. 2(f) ~ (i) show the surface current density and the magnetic field enhancement distributions of  $E'$ ,  $E$ ,  $m$  and  $M$ . In Fig. 2(b), the charges of the crescent and the cross oscillate in phase, so  $E'$  is a bright electric mode. Similarly, mode  $E$  is also a bright electric mode. Therefore, modes  $E'$  and  $E$  have a wide linewidth. In Fig. 2(e), the charges of crescent and cross oscillate out phase and the electric dipole moment is small. Two opposite current loops and magnetic hot spots are formed in the gap, so  $M$  is a dark magnetic mode. Destructive interference between the bright electric mode  $E$  and the dark magnetic mode  $M$  forms the magnetic Fano dip  $m$ . Fig. 2(d) and 2(h) show the charge distribution, magnetic field enhancement and surface current density distribution of dip  $m$ .

#### 3.2 New magnetic mode generation by rotating the cross

The optical properties of the CC with clockwise rotating

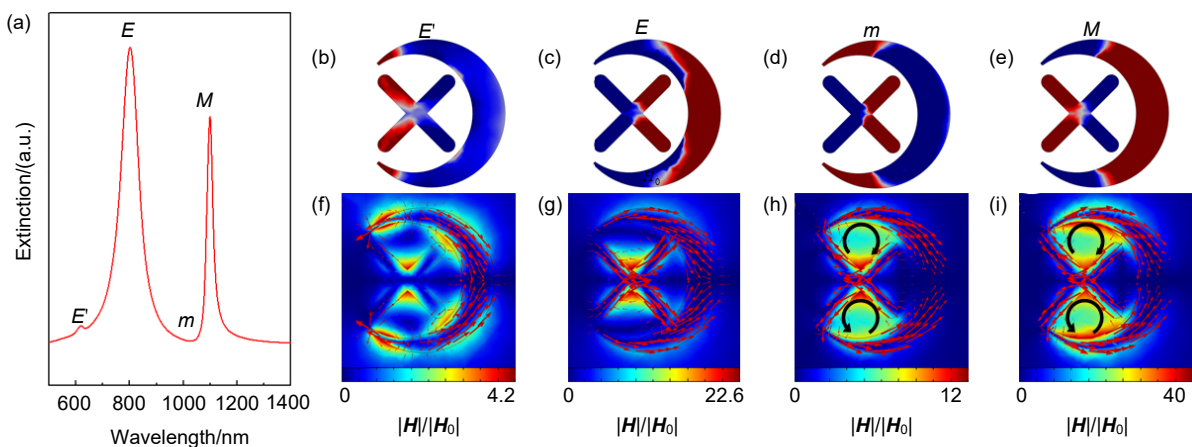


Fig. 2 (a) Extinction spectrum of the CC nanostructure; (b)~(e) The charge distributions; (f)~(i) The magnetic field enhancement and surface current density distributions of mode  $E'$ ,  $E$ ,  $m$  and  $M$ . Here,  $\mathbf{H}$  represents the local magnetic field, and  $\mathbf{H}_0$  represents the background magnetic field, where  $R=80$  nm,  $R_0=100$  nm,  $L=60$  nm,  $w=20$  nm and  $T=20$  nm

cross are further studied. Fig. 3(a) is the extinction spectra when the cross rotate angle is  $0^\circ$ ,  $10^\circ$ ,  $20^\circ$  and  $30^\circ$  respectively. When  $\theta$  is  $10^\circ$ , a new mode  $D$  appears near 950 nm, whose charge distribution is shown in Fig. 3(b). It can be seen that it is a quadrupole-quadrupole mode and the electric dipole moment is large. Fig. 3(c) shows the magnetic field enhancement and surface current density distributions of mode  $D$ . It can be seen that three circulations  $I_0$ ,  $I_1$ ,  $I_2$  and three hot spots are formed between the crescent and the cross. Therefore, mode  $D$  is bright magnetic mode, which is induced by the symmetry breaking of the CC nanostructure. The region of circulation  $I_2$  can be seen as a series of inductance and capacitance, the magnetic resonance at mode  $D$  is similar to LC resonance. The resonance frequency formula is showed by equation (1),

$$f = 1/\sqrt{LC} \quad (1)$$

here  $f$  is the resonance frequency,  $L$  is the inductance and  $C$  is the capacitance. As the rotating angle of the cross increases, the gap between the rod and the crescent is enlarged. The capacitance  $C$  decreases, and the resonance frequency  $f$  increases, so mode  $D$  blue shifts.

### 3.3 Double Fano resonance generation by rotating rod $a_2$

Rotating the rod  $a_2$  anticlockwise by  $15^\circ$ ,  $30^\circ$ ,  $45^\circ$  and  $60^\circ$ , the optical property of the CC nanostructure were further studied. For the symmetry breaking, a new mode  $G$  is created near 950 nm when  $\alpha$  is  $15^\circ$ . According to LC resonance frequency formula, as the rod  $a_2$  rotates anticlockwise, angle  $\alpha$  increases and the inductance  $L$  decreases, so the resonance frequency  $f$  increases and mode  $G$  blue shifts. At the same time, the distance between the two rods decreases, so the coupling between the two rods becomes stronger and the intensity of mode  $G$  is enhanced. Fig. 4(b) shows the charge distribution of mode  $G$ , which is a quadrupole-quadrupole mode with a small

electric dipole moment and can be judged as a dark mode. It's magnetic field enhancement and current distributions are shown in Fig. 4(c). Three hot spots and three circulations are formed between the crescent and the bars, so mode  $G$  is a dark magnetic mode. The dark magnetic mode  $G$  and the original bright electric mode  $E$  are coupled to form a Fano dip  $g$ . Fano dip  $g$  and  $m$  are called double Fano resonance.

### 3.4 Multiple Fano resonance generation by breaking structure symmetry

#### 3.4.1 Reducing the length of rod $a_1$

Fig. 5(a) shows the extinction spectra of the CC nanostructure when the half length of bar  $a_1$  reduces from 60 nm to 35 nm with 5 nm intervals. When  $L$  is 55 nm, a new mode  $V$  appears. When  $L$  is 50 nm, another new mode  $V'$  is induced, and when  $L$  is 45 nm, the third new mode  $B$  appears. Figs. 5(b)–5(d) show the charge distributions of the new modes  $B$ ,  $V'$ ,  $V$ . Figs. 5(e)–5(g) are magnetic field enhancements and surface current density distributions of the new modes  $B$ ,  $V'$ ,  $V$ . Fig. 5(d) shows that mode  $V$  is a dipole-quadrupole mode with a large electric dipole moment, which is a bright state. In Fig. 5(g), there are three current loops with opposite rotating directions and three magnetic hot spots in the gap between the crescent and the cross, so mode  $V$  is a bright magnetic mode. From Figs. 5(c) and 5(f), it can be seen that mode  $V'$  is a quadrupole-quadrupole mode, and the electric dipole moment is small, so it can be judged as dark mode. There is no circulation in the current distribution, so mode  $V'$  is a dark electric mode. The coupling of modes  $V$  and  $V'$  induces the first Fano dip  $b_2$  near 850 nm. Mode  $V'$  coupled with mode  $E$  to form the second electric Fano resonance dip  $b_1$  near 800 nm. From Figs. 5(b) and 5(e), it can be judged that mode  $B$  is also a dark mode. Mode  $B$  and  $E$  are coupled to form the third electric Fano resonance dip  $b$  at 680 nm. So,  $b$ ,  $b_1$  and  $b_2$  are the multiple Fano resonance.

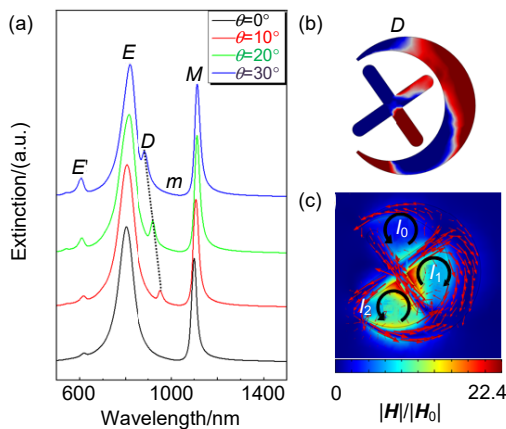


Fig. 3 (a) Extinction spectra of the CC nanostructure with rotating cross; (b) The charge distribution of the new mode  $D$  when  $\theta=10^\circ$ ; (c) The magnetic field enhancement and surface current density distribution of the new mode  $D$  when  $\theta=10^\circ$

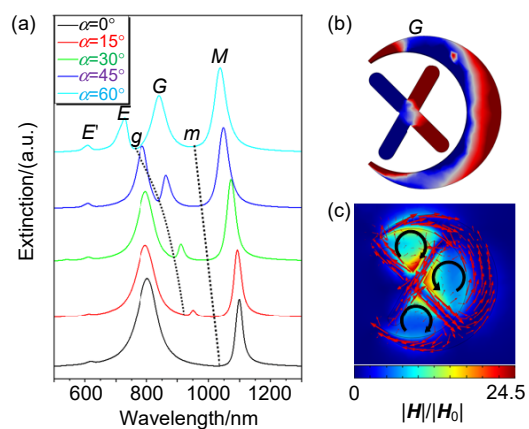


Fig. 4 (a) Extinction spectra of the CC nanostructure with rotating rod  $a_2$ ; (b) The charge distribution of mode  $G$  when  $\alpha=15^\circ$ ; (c) The magnetic field enhancement and current density distributions of mode  $G$  when  $\alpha=15^\circ$

### 3.4.2 Rotating the whole structure

The optical properties of the rotating CC nanostructure were studied. Fig. 6(a) shows the extinction spectra of the entire CC nanostructure with different rotating angle  $\beta$ . It can be seen that when  $\beta$  is  $15^\circ$ , new modes  $Z$  is generated. Continue to rotate the whole structure to  $30^\circ$ , new mode  $Z'$  appears. Then, rotate the whole structure to  $45^\circ$ , new mode  $H$  appears. Figs. 6(b)~6(d) are charge distributions of new modes  $Z'$ ,  $Z$  and  $H$ . Figs. 6(e)~6(g) are magnetic field enhancement and surface current density distributions of new modes  $Z'$ ,  $Z$ ,  $H$ . As shown in Figs. 6(b) and 6(e), a high-order quadrupole-octupole mode  $Z'$  is excited by rotating the overall structure, which can be judged as a bright electric mode. It can be seen from Figs. 6(c) and 6(f) that mode  $Z$  is a quadrupole-quadrupole mode and the electric dipole moment is small. There is no current loop in the structure, so it is judged to be a dark electric mode. Figs. 6(d) and 6(g) show that mode  $H$  is a quadrupole-quadrupole mode with a small electric dipole moment and three current loops, so mode  $H$  is a dark magnetic mode. Thus, the coupling of modes  $H$  and

$E$  induces the first magnetic Fano dip  $c_2$  at 900 nm. The coupling of modes  $E$  and  $Z$  produces the second Fano dip  $c_1$  at 700 nm. And the coupling of modes  $Z$  and  $Z'$  forms the third Fano dip  $c$  near 600 nm.  $c_2$ ,  $c_1$  and  $c$  are multiple Fano resonance.

As  $\beta$  increases, the intensity of mode  $M$  decreases continuously until the mode  $M$  disappears when  $\beta$  is  $90^\circ$ . This interesting phenomenon can be explained by Fig. 7. The black and red solid lines represent the symmetry axis of the CC nanostructure and the polarization direction of the electric field, respectively.  $\beta$  is the angle between the symmetry axis of the CC nanostructure and the polarization direction of the electric field. The polarization direction of the electric field can be decomposed along the symmetry axis ( $E_x$ ) of the CC structure and decomposed perpendicular to the symmetry axis ( $E_y$ ) (Fig. 7(b)). If  $\beta$  increases, the intensity of mode  $M$  will be reduced, which can be interpreted as the decrease of the parallel component  $E_x$ . When  $\beta$  is  $90^\circ$ , the mode  $M$  disappears because there is no parallel component  $E_x$  (Fig. 7(c)).

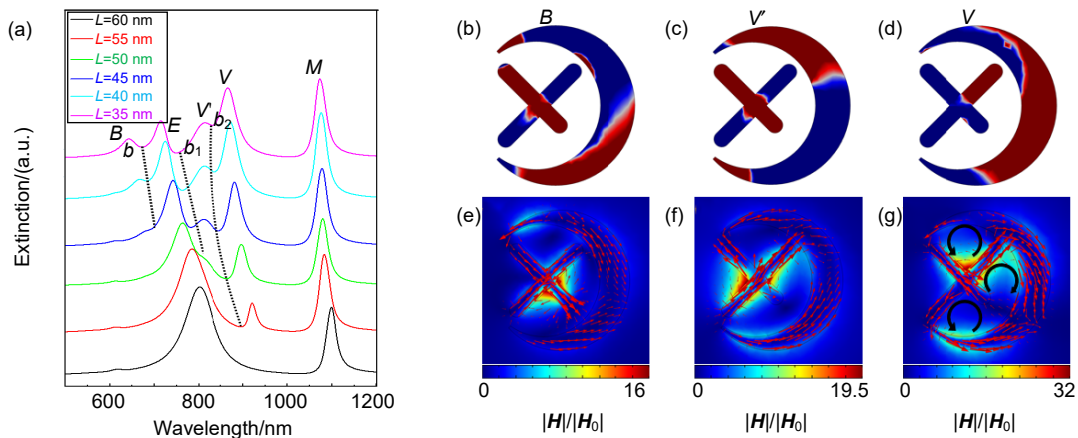


Fig. 5 (a) Extinction spectra of the CC nanostructure when bar  $a_1$  decreases; (b)~(d) The charge distributions of mode  $B$ ,  $V$ ,  $V$  when  $L=40$  nm; (e)~(g) The magnetic field enhancement and surface current density distributions of modes  $B$ ,  $V$ ,  $V$  when  $L=40$  nm

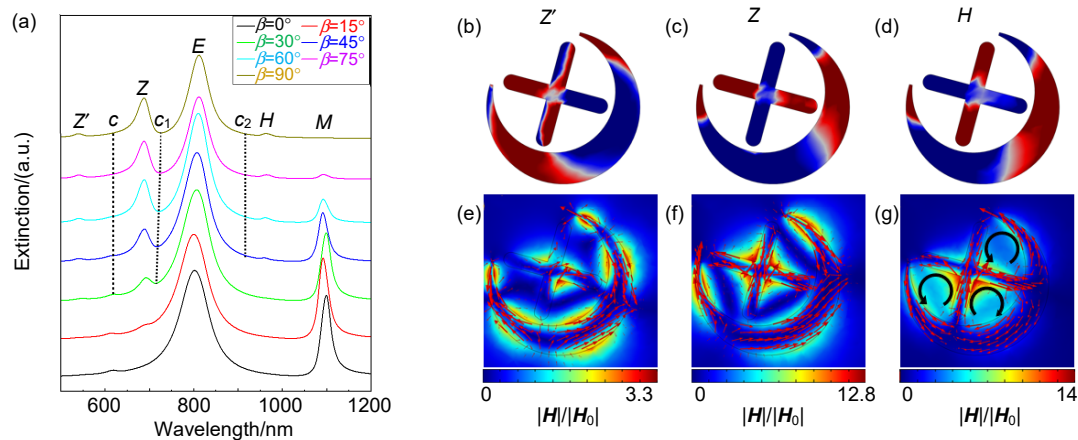


Fig. 6 (a) The extinction spectra of the CC nanostructure with rotating the whole structure from  $0^\circ$  to  $90^\circ$  with  $15^\circ$  intervals; (b)~(d) The charge distributions of mode  $Z'$ ,  $Z$  and  $H$  when  $\beta = 60^\circ$ ; (e)~(g) The magnetic field enhancement and surface current distributions of mode  $Z'$ ,  $Z$  and  $H$  when  $\beta = 60^\circ$

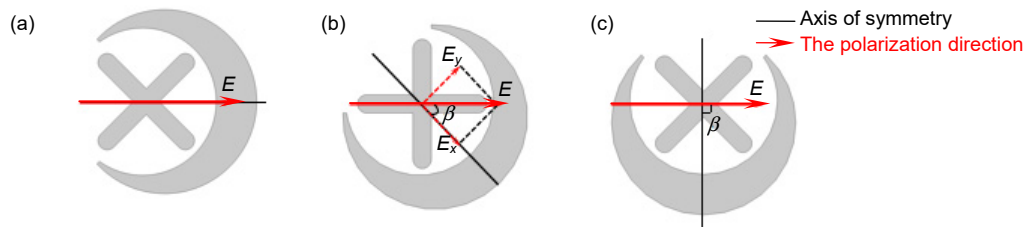


Fig. 7 Schematic diagram when the angle between the polarization direction of the electric field and the symmetry axis of the CC nanostructure  $\beta$  is (a)  $0^\circ$ ; (b)  $45^\circ$  and (c)  $90^\circ$  respectively.  $E_x$  and  $E_y$  are the parallel component and the vertical component of symmetry axis, respectively

### 3.5 High FOM by changing the angle between the two bars

The Fano resonance peak changes with the refractive index of the surrounding environment. As shown in Fig. 8(a), the extinction cross section and the resonance peak position of the CC nanostructure with different refractive index environments are simulated. The inset is the 2-D diagram of the structure, the angle between the two rods is  $150^\circ$ , and other parameters are the same as above. In order to study the sensitivity of the CC nanostructures to the surrounding environment, the position of mode  $M$  with different refractive index environments are calculated. When  $n$  is 1, mode  $M$  is at  $1090\text{ nm}$ , and when  $n$  is 1.05, mode  $M$  is red shifted to  $1140\text{ nm}$ , which is due to the influence of environmental change on far-field interference between different scatter paths. As we all know, device sensitivity is an important indicator for the performance of a sensor, which is calculated by the formula (2),

$$S = \delta\lambda / \delta n \quad (2)$$

here  $S$  is the refractive index sensitivity, and  $\delta\lambda$  represents the difference in peak positions at two different refractive indices.  $\delta n$  represents the difference between the refractive indices of the two environments. Here, the refractive index change of the environment is 0.05, and the refractive index sensitivity of the mode  $M$  is  $1000\text{ nm/RIU}$ . In addition, FOM is also an important indicator for the performance of a sensor, which is calculated by the formula (3),

$$V_{\text{FOM}} = \frac{S}{W_{\text{FWHM}}} \quad (3)$$

the  $W_{\text{FWHM}}$  is the full width at half maximum of the resonance mode, the  $V_{\text{FOM}}$  of the CC nanostructure is 61.

The FOM was studied when change the angle between two rods in a metal nanostructure. Fig. 8(b) shows that, as the angle between the two rods changes from  $90^\circ$  to  $180^\circ$  with  $15^\circ$  intervals, the FOM value increases firstly and then reduces sharply to 35 at  $165^\circ$  and finally increases to 48 at  $180^\circ$ . It can be found that the highest FOM value is 61. Compared with other plasma metal nanostructures, the FOM value of the CC metal nanostructures studied in this paper is relatively high, and it has applications in biosensors, optical switches, photodetectors, etc.

## 4 Conclusions

We designed a CC nanostructure to achieve multiple Fano resonance with high FOM magnetic resonance. Breaking the symmetry of the structure by rotating the cross and the single rod, a new magnetic mode can be created. The multiple Fano resonance can be generated by rotating the whole structure and reducing the length of rod  $a_1$ . High FOM can be implemented by changing the angle between the two rods in the structure. These excellent optical properties make the CC nanostructures have potential application prospects in ultra-sensitive biosensors, surface enhanced spectroscopy and so on.

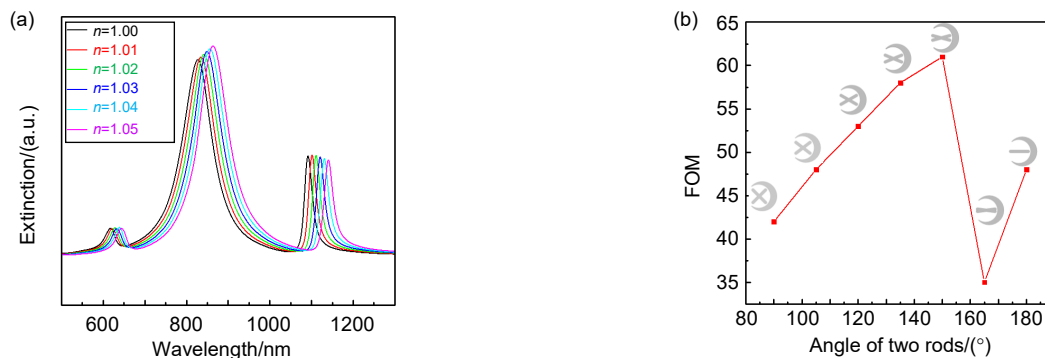


Fig. 8 (a) The extinction cross-section of the CC nanostructures varies with the refractive index of the surrounding environment. The angle between the two rods is  $150^\circ$ ; (b) The FOM value of the structure changing with the angle between the two rods

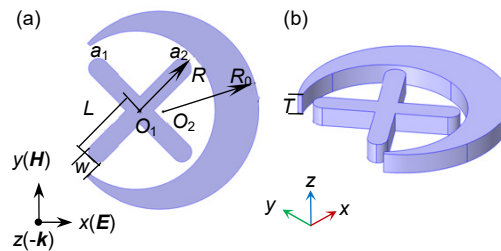
## References

- [1] Zhang J X, Zhang L D. Nanostructures for surface plasmons[J]. *Advances in Optics and Photonics*, 2012, **4**(2): 157–321.
- [2] Gao W T, Chen C Y, Sun Z J. Local field enhancement and its wavelength tuning in metal nanoparticle arrays[J]. *Japanese Journal of Applied Physics*, 2019, **58**(3): 030910.
- [3] Garcia M A. Surface plasmons in metallic nanoparticles: fundamentals and applications[J]. *Journal of Physics D: Applied Physics*, 2011, **44**(28): 283001.
- [4] Lodewijks K, Ryken J, Van Roy W, et al. Tuning the fano resonance between localized and propagating surface plasmon resonances for refractive index sensing applications[J]. *Plasmonics*, 2013, **8**(3): 1379–1385.
- [5] Newman D M, Wears M L, Matelon R J, et al. Magneto-optic behaviour in the presence of surface plasmons[J]. *Journal of Physics Condensed Matter*, 2008, **20**(34): 345230.
- [6] Liu L, Han Z H, He S L. Novel surface plasmon waveguide for high integration[J]. *Optics Express*, 2005, **13**(17): 6645–6650.
- [7] Dong J, Qu S X, Zheng H R, et al. Simultaneous SEF and SERRS from silver fractal-like nanostructure[J]. *Sensors and Actuators B: Chemical*, 2014, **191**: 595–599.
- [8] Ooi C H R, Tan K S. Controlling double quantum coherence and electromagnetic induced transparency with plasmonic metallic nanoparticle[J]. *Plasmonics*, 2013, **8**(2): 891–898.
- [9] Luk'Yanchuk B, Zheludev N I, Maier S A, et al. The fano resonance in plasmonic nanostructures and metamaterials[J]. *Nature Materials*, 2010, **9**(9): 707–715.
- [10] Kobayashi K, Aikawa H, Sano A, et al. Fano resonance in a quantum wire with a side-coupled quantum dot[J]. *Physical Review B*, 2004, **70**(3): 035319.
- [11] de Guevara M L L, Claro F, Orellana P A. Ghost fano resonance in a double quantum dot molecule attached to leads[J]. *Physical Review B*, 2003, **67**(19): 195335.
- [12] Hajebifard A, Berini P. Fano resonances in plasmonic heptamer nano-hole arrays[J]. *Optics Express*, 2017, **25**(16): 18566–18580.
- [13] Fang Z Y, Liu Z, Wang Y M, et al. Graphene-antenna sandwich photodetector[J]. *Nano Letters*, 2012, **12**(7): 3808–3813.
- [14] Fang Z Y, Cai J Y, Yan Z B, et al. Removing a wedge from a metallic nanodisk reveals a fano resonance[J]. *Nano Letters*, 2011, **11**(10): 4475–4479.
- [15] Frimmer M, Coenen T, Koenderink A F. Signature of a fano resonance in a plasmonic metamolecule's local density of optical states[J]. *Physical Review Letters*, 2012, **108**(7): 077404.
- [16] Chen S, Meng L Y, Hu J W, et al. Fano interference between higher localized and propagating surface plasmon modes in nanovoid arrays[J]. *Plasmonics*, 2015, **10**(1): 71–76.
- [17] Li J, Zhang Y, Jia T Q, et al. High tunability multipolar fano resonances in dual-ring/disk cavities[J]. *Plasmonics*, 2014, **9**(6): 1251–1256.
- [18] Kuznetsov M, Haus H. Radiation loss in dielectric waveguide structures by the volume current method[J]. *IEEE Journal of Quantum Electronics*, 1983, **19**(10): 1505–1514.
- [19] Huo Y Y, Jia T Q, Zhang Y, et al. Spaser based on fano resonance in a rod and concentric square ring-disk nanostructure[J]. *Applied Physics Letters*, 2014, **104**(11): 113104.
- [20] Zhao Q, Yang Z J, He J. Fano resonances in heterogeneous dimers of silicon and gold nanospheres[J]. *Frontiers of Physics*, 2018, **13**(3): 137801.
- [21] Lee K L, Wu S H, Lee C W, et al. Sensitive biosensors using fano resonance in single gold nanoslit with periodic grooves[J]. *Optics Express*, 2011, **19**(24): 24530–24539.
- [22] Lee E, Zhou K, Gwon M, et al. Surface plasmon-induced absorption enhancement of silicon nanowire array[J]. *Proceedings of SPIE*, 2012, **8457**: 84572C.
- [23] Tasolamprou A C, Zografopoulos D C, Kriezis E E. Liquid crystal-based dielectric loaded surface plasmon polariton optical switches[J]. *Journal of Applied Physics*, 2011, **110**(9): 093102.
- [24] Gong X, Tong M H, Xia Y J, et al. High-detectivity polymer photodetectors with spectral response from 300 nm to 1450 nm[J]. *Science*, 2009, **325**(5948): 1665–1667.
- [25] Berini P. Surface plasmon photodetectors and their applications[J]. *Laser & Photonics Reviews*, 2014, **8**(2): 197–220.
- [26] Bao Y J, Hu Z J, Li Z W, et al. Magnetic plasmonic fano resonance at optical frequency[J]. *Small*, 2015, **11**(18): 2177–2181.
- [27] Bao Y J, Zu S, Zhang Y F, et al. Active control of graphene-based unidirectional surface plasmon launcher[J]. *ACS Photonics*, 2015, **2**(8): 1135–1140.
- [28] Bao Y J, Zhu X, Fang Z Y. Plasmonic toroidal dipolar response under radially polarized excitation[J]. *Scientific Reports*, 2015, **5**: 11793.
- [29] Zhang Q, Wen X L, Li G Y, et al. Multiple magnetic mode-based fano resonance in split-ring resonator/disk nanocavities[J]. *ACS Nano*, 2013, **7**(12): 11071–11078.
- [30] Yang L, Wang J C, Yang L Z, et al. Characteristics of multiple fano resonances in waveguide-coupled surface plasmon resonance sensors based on waveguide theory[J]. *Scientific Reports*, 2018, **8**(1): 2560.
- [31] Kong Y, Cao J J, Qian W C, et al. Multiple fano resonance based optical refractive index sensor composed of micro-cavity and micro-structure[J]. *IEEE Photonics Journal*, 2018, **10**(6): 6804410.
- [32] Li C, Li S L, Wang Y L, et al. Multiple fano resonances based on plasmonic resonator system with end-coupled cavities for high-performance nanosensor[J]. *IEEE Photonics Journal*, 2017, **9**(6): 4801509.
- [33] Zhang Y Y, Li S L, Zhang X Y, et al. Evolution of fano resonance based on symmetric/asymmetric plasmonic waveguide system and its application in nanosensor[J]. *Optics Communications*, 2016, **370**: 203–208.
- [34] Yun B F, Hu G H, Cong J W, et al. Fano resonances induced by strong interactions between dipole and multipole plasmons in t-shaped nanorod dimer[J]. *Plasmonics*, 2014, **9**(3): 691–698.
- [35] Wang J Q, Fan C Z, He J N, et al. Double fano resonances due to interplay of electric and magnetic plasmon modes in planar plasmonic structure with high sensing sensitivity[J]. *Optics Express*, 2013, **21**(2): 2236–2244.
- [36] Gonçalves M R, Melikyan A, Minassian H, et al. Strong dipole-quadrupole coupling and fano resonance in h-like metallic nanostructures[J]. *Optics Express*, 2014, **22**(20): 24516–24529.

# Generation of multiple Fano resonance and high FOM resonance based on the crescent cross nanostructure

Hou Yibo, Huo Yiping\*, Jiang Xueying, Zhou Chen, Guo Yiyuan,  
Niu Qiqiang, He Qian, Hao Xiangxiang

School of Physics and Information Technology, Shaanxi Normal University, Xi'an, Shaanxi 710062, China



(a) 2-D structure and geometric parameters of the CC nanostructure; (b) 3-D schematic diagram of the CC nanostructure

**Overview:** In recent years, great progress has been made in the research based on surface plasmons (SPs). SPs has been widely used in nano-optoelectronic integration, optical imaging, biosensor, data storage, and has attracted great attention of researchers. Fano resonance comes from the quantum system originally. When the discrete and the continuous energy level are superimposed, quantum interference occurs and low absorption happens at a specific optical frequency, which results in an asymmetric linetype. U Fano explained the mechanism of asymmetric linetype by using strict theory. In the SPs system, Fano resonance can be formed by the coupling between the bright mode (superradiant) and the dark mode (subradiant), which results in the asymmetric spectrum. Fano resonance is characterized by asymmetric linetype. A spectral dip is formed through coupling of bright mode and dark mode, where scattering is suppressed and absorption is enhanced. In order to explore the optical characteristics and application of surface plasmon resonance modes of composite metal nanostructures, a crescent cross (CC) nanostructure composed of a crescent and a cross is designed. A commercial software COMSOL Multiphysics based on the finite element method is used to calculate the optical response of the CC nanostructure. The direction of incident light is perpendicular to the surface of the nanostructure, and the polarization of light propagates parallel to the structure. By changing the structural parameters to break the symmetry of the nanostructure, rich optical properties can be obtained. The rotating cross can excite the surface plasmon resonance magnetic mode, and the electric mode and the magnetic mode are coupled to form the magnetic Fano resonance. The magnetic Fano resonance has advantages that the electrical Fano resonance does not have. A closed-loop current can be formed, which can limit the energy more locally, reduce the scattering loss and strengthen the response of the magnetic field. By rotating and shortening the single rod  $a_2$ , the structural symmetry is broken to generate multiple Fano resonance effects. Meanwhile, the optical characteristics of the plasmon resonance mode on the surface of the nanostructure are tuned by changing the polarization direction of light (rotating the entire structure) without changing the basic structure, and it is found that new Fano resonances occur continuously during the rotation process, thus forming multiple Fano resonances. In order to explore the application potential of crescent cross nanostructure in sensing field, we calculated its sensitivity. By changing the angle between the two rods symmetrically, the figure of merit (FOM) can reach 61. Our structure has important applications in the fields of multi-wavelength sensor, ultra-sensitive biosensor, surface enhanced spectroscopy and slow light transmission.

**Citation:** Hou Y B, Huo Y P, Jiang X Y, *et al.* Generation of multiple Fano resonance and high FOM resonance based on the crescent cross nanostructure[J]. *Opto-Electronic Engineering*, 2020, 47(11): 200010

Supported by National Natural Foundation of China (11604198)

\* E-mail: yphuo@snnu.edu.cn